Pergamon

Int. J. Heat Mass Transfer. Vol. 38, No. 13, pp. 2353–2366, 1995

0017-9310/95 $9.50+0.00

0017-9310(94)00360-2

Numerical studies of forced convection heat transfer from a cylinder embedded in a packed bed

K. J. NASR,† S. RAMADHYANI‡ and R. VISKANTA

School of Mechanical Engineering Purdue University West Lafayette, IN 47907, U.S.A.

(*Received* 4 *April* 1994 *and in final form* 1 *December* 1994)

Abstract—Forced convection heat transfer from a cylinder embedded in a packed bed was studied numerically. The local volume-averaged conservation equations were used to examine the effects of the governing dimensionless parameters: the Reynolds, Darcy, Forchheimer and effective Prandtl numbers. An increase in either the Reynolds number or effective Prandtl number resulted in heat transfer enhancement. The effect of decreasing Darcy number (*Da*) was an increase in the Nusselt number. The effect of Forchheimer number on heat transfer was found to depend on the product of Darcy and Reynolds numbers ($Da\,Re_D$). Through a comparison of numerical predictions with experimental data, effective conductivities were extracted and average thermal dispersion effects were quantified.

INTRODUCTION

An effective technique for enhancing convective heat transfer is to embed the heat transfer surface in a packed bed. The heat transfer enhancement is due to the combined effects of the reduced boundary layer thickness and increased fluid mixing (thermal dispersion) produced by the porous medium. The enhancement in heat transfer is, of course, achieved at the expense of additional pressure drop. The present paper reports the results of a numerical study of forced convective heat transfer from a circular cylinder embedded in a packed bed of spherical particles. The objectives of this study are to examine the effects of various governing parameters and to compare the numerical predictions with the results of the boundary-layer theory and with experimental data. Additional motivation for this study stems from the fact that few comparisons of numerical predictions with experimental data have been presented by previous investigators. Such a comparison has been used in this study to postulate and quantify a dispersive contribution to the effective thermal conductivity of the porous medium. The dispersive thermal conductivity has been calculated by subtracting the stagnant thermal conductivity from the effective thermal conductivity required to produce a match between the model predictions and the experimental data.

Theoretical studies (Cheng [1]; Minkowycz *et al.* [2]) considered heat transfer to or from a cylinder in a packed bed, employing the boundary layer approximation to the energy equation in conjunction with Darcy's flow model. Numerical studies based on Darcy flow were presented by Huang *et al.* [3] and Badr and Pop [4]. A numerical study, accounting for non-Darcian effects, was performed by Murty *et al.* [5] who concluded that heat transfer from an embedded cylinder was weakly dependent on Darcy and Forchheimer numbers for $Da < 10^{-4}$ and $Re_p < 200$. Fand and Phan [6], Fand *et al.* [7], and Nasr *et al.* [8] reported experimental data on average heat transfer coefficients along with various forms of semi-empirical correlations to predict the average Nusselt number. An expression for the variation of the local Nusselt number over an isothermal cylinder embedded in porous media with forced flow was given by Cheng [1]:

$$Nu_\theta = 0.5641\, Pe_\theta^{0.5} \sqrt{(2\theta)} \sin\theta (1-\cos\theta)^{-0.5}. \quad (1)$$

Averaging of the local Nusselt number over the cylinder surface yields an expression for the average Nusselt number:

$$\overline{Nu_D} = 1.0157\, Pe_D^{1/2}. \quad (2)$$

In these expressions, the Nusselt and Peclet numbers are based on an effective (volume-averaged) thermal conductivity of the porous medium.

PROBLEM FORMULATION

Most of the early studies employed Darcy's law (applicable when $Re_p < 1$) to model fluid flow through packed beds. However, many systems of current interest involve higher Reynolds numbers as well as impermeable boundaries to confine the flow and the porous medium. Hence, inclusion of inertia and boundary effects is necessary for improved modeling of the

† Present address: GMI Engineering & Management Institute, Flint, MI 48504, U.S.A.

‡ Author to whom correspondence should be addressed.

NOMENCLATURE

A, B	Ergun constants
C_{disp}	average coefficient of thermal dispersion
c_p	specific heat of the fluid
D	cylinder diameter
Da	Darcy number, K/D^2
d_p	particle diameter
F	inertial coefficient
Fs	Forchheimer number, $F D/K^{1/2}$
H	extent of the packed bed in the x-direction
h	average heat transfer coefficient of the embedded cylinder
h_{Exp}	experimental average heat transfer coefficient
h_{Num}	numerical average heat transfer coefficient obtained from FIDAP
K	permeability of the porous medium
k_o	extrapolated value of effective conductivity for zero Peclet number
k_{disp}	dispersive conductivity
k_{eff}	effective thermal conductivity
k_f	thermal conductivity of the fluid
k_m	stagnant effective thermal conductivity of the porous medium
L	extent of the packed bed in the y-direction
Nu_D	cylinder averaged Nusselt number, $h D/k_{eff}$
Nu_θ	local Nusselt number on the cylinder surface, $q_w R\theta/k_{eff}(T_s - T_i)$
Pe_D	average Peclet number, $U_\infty D/\alpha_{eff}$
Pe_p	particle Peclet number, $U_\infty d_p/\alpha_f$
Pe_θ	local Peclet number on the cylinder surface, $U_\infty D\theta/2\alpha_m$
Pr_{eff}	effective Prandtl number, $(\mu c_p)_f/k_{eff}$
R	radius of the cylinder
Re_D	Reynolds number, $\rho U_\infty D/\mu$
Re_D'	Reynolds number using the effective viscosity, $\rho U_\infty D/\mu'$
Re_p	Reynolds number based on the particle diameter, $\rho U_\infty d_p/\mu$
T_i	temperature of the approaching fluid
T_s	cylinder surface temperature
U	dimensionless x-direction velocity component
u	x-direction component of Darcy's filtration velocity
U_∞	velocity of the approaching fluid
$\mathbf{V}$	Darcian volume-averaged velocity vector
V	dimensionless y-direction velocity component
v	y-direction component of Darcy's filtration velocity.

Greek symbols

α	thermal diffusivity
α_{eff}	effective thermal diffusivity of the porous bed, $k_{eff}/\rho c_p$
α_f	thermal diffusivity of the saturating fluid, $k_f/\rho c_p$
α_m	stagnant effective thermal diffusivity of the porous bed, $k_m/\rho c_p$
β	coefficient of volumetric expansion of the fluid
Θ	dimensionless temperature, $(T - T_i)/(T_s - T_i)$
θ	angle measured from forward stagnation point
μ	dynamic viscosity of the fluid
μ'	effective viscosity in the Brinkman term
ν	kinematic viscosity of the fluid
ϕ	bulk porosity of the packed bed (porous medium)
ρ	density of the fluid.

Superscript

$\bar{}$	average value.

physical phenomena. These effects are normally accounted for by modifying Darcy's law, i.e. adding a quadratic term in velocity (inertia effect) and viscous shearing stress terms (boundary effect) in the momentum equations. The inclusion of shear stress terms is known as Brinkman's extension, and the quadratic inertia term is known as Forchheimer's extension. In addition to these extensions of the momentum equations, thermal dispersion effects become important at high velocities and are accounted for through the use of a total effective thermal conductivity in the energy equation. In this paper, the aforementioned physical mechanisms, non-Darcian effects and thermal dispersion, will be analyzed and highlighted through numerical simulations.

Application of a volume-averaging technique (Slattery [9]; Vafai and Tien [10]; Carbonell and Whitaker [11]; Hsu and Cheng [12]; Kaviany [13]) to the fundamental microscopic transport equations in a porous medium results in a system of conservation equations on a macroscopic scale. In terms of the Darcian velocity and on a macroscopic scale, these local volume-averaged equations take on the following form [12]:

Continuity

$$\nabla \cdot (\mathbf{V}) = 0 \tag{3}$$

Momentum

$$\frac{\rho_f}{\phi}(\mathbf{V}\cdot\nabla)\mathbf{V} = -\nabla p + \mu'\nabla^2\mathbf{V} - \left[\frac{\mu_f}{K}\phi\mathbf{V} + \frac{\rho_f}{\sqrt{K}}F\phi\mathbf{V}|\mathbf{V}|\right] \tag{4}$$

Energy

$$\rho_f c_{p_f}(\mathbf{V}\cdot\nabla)T = \nabla\cdot(k_{\text{eff}}\nabla T) \tag{5}$$

where $\mathbf{V}$ is the Darcian velocity vector, $\mathbf{V} = \phi\mathbf{V}_f$. The volumetric average fluid phase velocity vector is $\mathbf{V}_f$, and $p = \phi\, p_f$, where p_f is the volumetric average pressure of the fluid. Each term and its relative magnitude in the momentum equation is discussed in detail in Nasr [18]. The term appearing on the left-hand side (LHS) of the momentum equation represents macroscopic inertia. It is usually less important when compared to the terms on the RHS, except near the wall where the Brinkman frictional effect predominates (Lauriat and Vafai [14]). Nield and Bejan [15] presents an argument in favor of discarding this term and recommend the use of the Forchheimer drag term (quadratic in velocity) to account for the overall non-linear inertia effects.

The assumptions made in establishing these equations are: (1) The flow is steady and incompressible, (2) the solid matrix is in thermal equilibrium with the fluid, (3) the viscous heat dissipation and volumetric heat generation are negligible and (4) the thermophysical properties are independent of temperature.

The empirical and semi-empirical correlations used for the permeability and the inertial coefficient in conjunction with the foregoing governing equations are given below. As advanced by Ergun [16], Kozeny related the permeability to the bed porosity by modeling the porous medium as a collection of solid spheres of diameter d_p, and proposed that

$$K = \frac{\phi^3 d_p^2}{A(1-\phi)^2}. \tag{6}$$

The inertia coefficient, F, was shown to depend on the porosity and Ergun's coefficients A and B:

$$F = \frac{B\phi^{-1.5}}{\sqrt{A}}. \tag{7}$$

The values employed for the Ergun coefficients, A and B, are 220 and 1.6, respectively.

It should be noted that the foregoing conservation equations are for forced convection flow and do not account for any buoyancy effects. In the present study, natural convection effects are expected to be negligible since the Rayleigh number based on the permeability and cylinder diameter, $Ra_m = g\,\beta\,\Delta\,T\,K\,D/\nu_f\alpha_m$, is of the order of 0.05.

DIMENSIONLESS EQUATIONS

The governing equations may be non-dimensionalized using the following variables:

$$X = \frac{x}{D} \quad Y = \frac{y}{D} \quad U = \frac{u}{U_\infty} \quad V = \frac{v}{U_\infty}$$

$$\Theta = \frac{T-T_i}{T_s-T_i} \quad \text{and} \quad P = \frac{p}{\rho U_\infty^2}.$$

On making appropriate substitutions in the dimensional equations, we get:

$$\frac{\partial U}{\partial X} + \frac{\partial V}{\partial Y} = 0 \tag{8}$$

$$\frac{1}{Da\,Re_D}U + Fs|\mathbf{V}'_m|U = -\frac{\partial P}{\partial X} + \frac{1}{Re'_D}\nabla^2 U \tag{9}$$

$$\frac{1}{Da\,Re_D}V + Fs|\mathbf{V}'_m|V = -\frac{\partial P}{\partial Y} + \frac{1}{Re'_D}\nabla^2 V \tag{10}$$

$$U\left(\frac{\partial\Theta}{\partial X} + \frac{\partial\Theta}{\partial Y}\right) = \frac{1}{Re_D Pr_{\text{eff}}}\nabla^2\Theta \tag{11}$$

where $|\mathbf{V}'_m| = \sqrt{U^2+V^2}$.

In this study the effective Reynolds number, based on the effective viscosity, is taken to be equal to the Reynolds number based on the dynamic viscosity.

A parametric study to examine the effect of each of the dimensionless parameters on heat transfer was undertaken. In addition, a comparison between numerical predictions and experimental data was performed and used as a basis for quantifying thermal dispersion effects. Owing to symmetry, the computational domain was taken to be half of the physical domain. Figure 1(a) is a schematic of the computational problem with the appropriate velocity and temperature boundary conditions. It was assumed that the confining walls were adiabatic and sufficiently far from the surface of the embedded cylinder ($L = 6D$) to render any influence on heat transfer negligible. The boundary conditions for U, V and Θ are:

Cylinder surface	$U = V = 0$ and $\Theta = 1$
Domain inlet	$U = 1, V = 0$ and $\Theta = 0$
Confining wall	$U = V = 0$
Symmetry plane	$V = 0$.

VALIDATION OF NUMERICAL PREDICTIONS

In the present numerical study, the conservation equations were solved using the general-purpose finite element program FIDAP (FDI [17]), which employs a Galerkin-based finite element method. Prior to generating the numerical results reported in this paper, grid-independence of the results was assessed and the predictions were validated against an available analytical solution.

The mesh discretizing the computational domain consisted of 1300 nine-noded elements, and is shown in Fig. 1(b). It is a result of a grid refinement study that was conducted at $Re_D = 2800$ and $Da = 2.0\times10^{-4}$ by progressively increasing the number of elements until no noticeable change in the predicted value of the heat transfer coefficient was observed. Fifty nodes were considered appropriate on the half-cylinder surface since the discretized approximation to the arc length

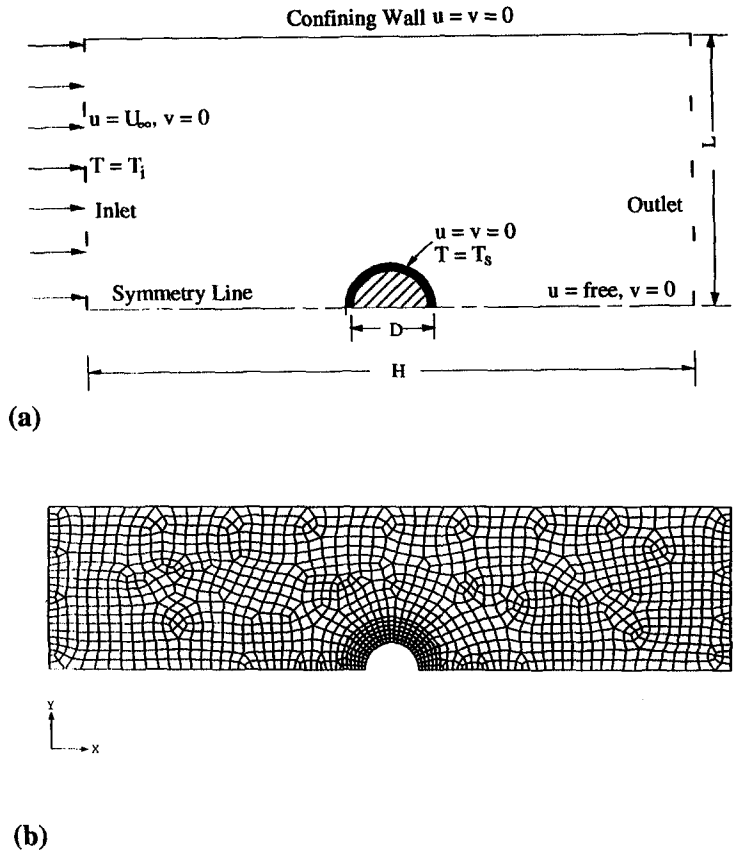

Fig. 1. (a) The computational domain of the physical system and associated boundary conditions and (b) the mesh used for the numerical simulations

was computed to be within 0.05% of the actual dimension of the half-cylinder perimeter ($\pi D/2$). A detailed discussion of the grid refinement study has been presented by Nasr [18]. The layer of boundary elements around the cylinder is introduced to capture sharp gradients of velocity and temperature in the boundary layer around the cylinder.

The numerical solution of the model equations obtained by FIDAP may be compared to, and validated against, the boundary-layer solution in conjunction with the Darcy flow model, equation (2). The flow is considered to be in the Darcy regime when the Reynolds number based on the particle diameter is less than 1 (Fand *et al.* [7]). In the Darcy regime, thermal dispersion effects may be neglected, and the effective thermal conductivity is equivalent to the stagnant conductivity. For the simulation of flow and heat transfer in glass–air and glass–water packed beds, the Darcy number was taken as 1×10^{-4}. Stagnant conductivities for glass–air and glass–water beds were obtained using the model of Zehner and Schlünder [19]. The values employed for the effective Prandtl number of the glass–air and glass–water packed beds were 0.10 and 0.023, respectively. Quantitatively, the deviation between the numerical predictions and the boundary layer solution is approximately 2% for low Re_D and 7% for high Re_D. Therefore, the predictions were considered to agree well with each other, and the numerical results based on FIDAP were considered to be acceptable.

Since an analytical solution for heat transfer incorporating the Darcy–Brinkman–Forchheimer formulation is unavailable, a direct validation of the numerical model for that case could not be performed. However, in addition to the comparison with the boundary-layer theory predictions, various numerical simulations under isothermal conditions were performed to insure the proper computation of pressure drop. As described in detail in Nasr [18], the pressure drop predicted by the Darcy–Brinkman–Forchheimer formulation of the momentum equations was in excellent agreement with measured values. These pressure drops may be easily computed from a reduced form of the streamwise momentum equation in which the velocity distribution is considered to be uniform in the channel cross section.

NUMERICAL RESULTS AND DISCUSSION

In order to illustrate the effects of the Brinkman and Forchheimer extensions of the momentum equation, numerical simulations were carried out for a Darcy

(no inertia or boundary effects), Darcy–Brinkman (no inertia effects), and Darcy–Brinkman–Forchheimer momentum equation (all effects included). Figure 2 illustrates the local predicted Nusselt number as a function of angular location measured from the forward stagnation point, along with the predictions of the boundary layer analysis expression, equation (1). The results show that the addition of the Brinkman term to the Darcy momentum equation resulted in a slight decrease in heat transfer (4% decrease in the average Nusselt number value). Inclusion of the Forchheimer term in the momentum equation was found to cause a more noticeable change in the local Nusselt number variation and resulted in a decrease of 3% in the average Nusselt number, relative to the Darcy momentum equation. The fluid velocity is relatively high (2 m s^{-1}) yielding large inertia effects relative to Darcy and Brinkman effects and causing the local variation in Nusselt number. An examination of the heat transfer characteristics by considering the effect of each of the dimensionless numbers in the transport equations is presented next. The predictions are based on the extended Darcy–Brinkman–Forchheimer momentum equations.

Effect of Reynolds number—flow velocity

Any increase in the cylinder-based Reynolds number would enhance heat transfer and cause an increase in the average Nusselt number value, $h\,D/k_{\text{eff}}$. For a fixed value of effective Prandtl number, an increase of Reynolds number from a value of 50 to a higher value of 2000, causes an increase in the Nusselt number by a factor of five and a half. This increase agrees closely with the prediction of the boundary layer theory, which yields $Nu_D \sim Re_D^{1/2}$.

Figure 3 shows the effect of the Reynolds number on the temperature profile at an angular location of 90°. It is evident that the temperature profile at a $Re_D = 2$ is substantially different from that at $Re_D = 50$ and that the temperature profiles at $Re_D = 50$ are closer to those associated with the higher Reynolds number flows. When $Re_D > 1000$, the temperature drops from its wall value to its free stream value within a distance of only half the cylinder radius.

Effect of Darcy number—permeability effect

The Darcy number is directly proportional to the bed permeability. For a fixed cylinder diameter, different values of Darcy number correspond to different permeabilities for the porous medium. The permeability is bed-structure dependent and is commonly formulated in terms of particle diameter and bed porosity. From the momentum equation, one may deduce that as the permeability increases and approaches a very large value, equation (9) approaches the form of the Navier–Stokes equation.

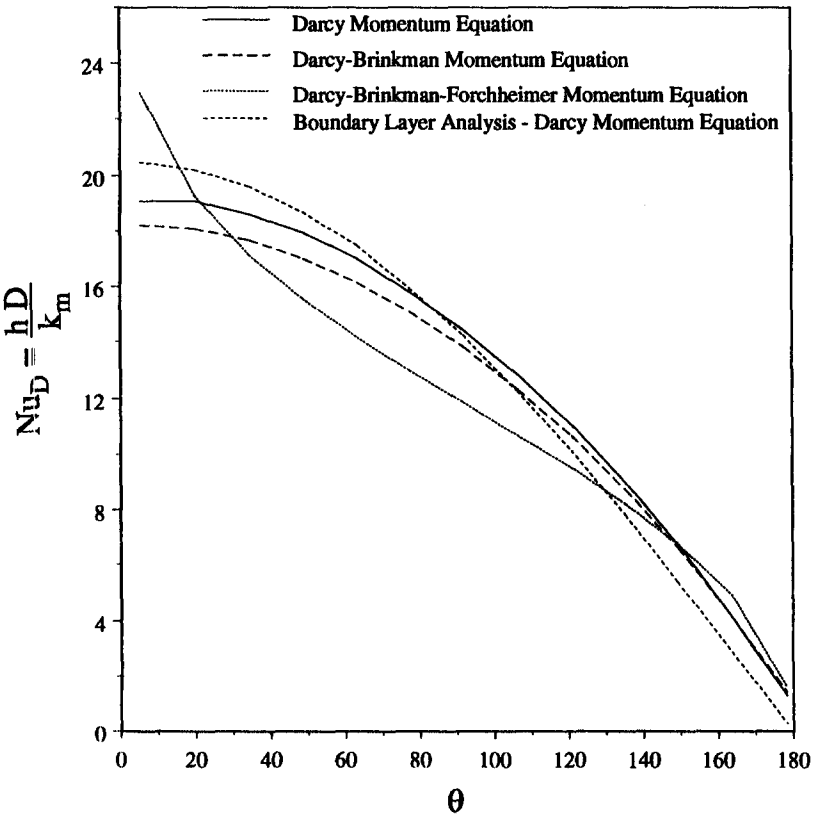

Fig. 2. Variation of Nusselt number over an embedded cylinder for a Darcy–Brinkman–Forchheimer flow, $Re_D = 1500$, $Da = 1 \times 10^{-4}$, $Pr_{\text{eff}} = 0.1$ and for the Darcy–Brinkman–Forchheimer equation $Fs = 50$.

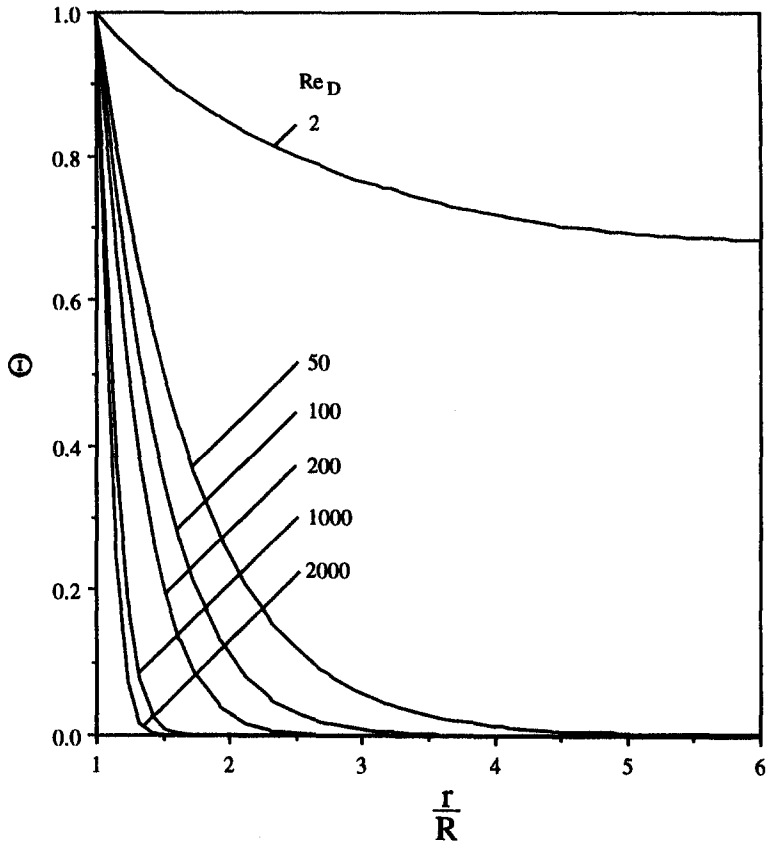

Fig. 3. Temperature profiles at an angular location of 90° for a range of Reynolds number values, $Da = 1 \times 10^{-4}$, $Fs = 50$ and $Pr_{eff} = 0.1$.

In order to examine the effect of this parameter on heat transfer, numerical simulations were performed for a wide range of Darcy numbers. As the Darcy number increases, heat transfer from the cylinder decreases. Table 1 summarizes the tabulated values of the average Nusselt number which correspond to increasing values of Darcy number from 1×10^{-4} to 1. For convenience, the values of permeability and computed heat transfer coefficients are also tabulated. A four-order of magnitude increase in *Da* results in approximately 35% decrease in the average Nusselt number. Although a decrease in the Darcy number yields an increase in the Nusselt number, the rate of this increase in *Nu* decreases with decreasing values of *Da*.

Figure 4 presents the variation of local Nusselt number over half of the circumference of the cylinder. The effect of higher values of *Da* is especially pronounced over the front 90 degrees of the cylinder surface and shows that lower Nusselt numbers are obtained for the higher *Da* values. In essence, the effect of increasing *Da* is a decrease of heat transfer from the cylinder.

Effect of Forchheimer number—inertia effects

It was previously noted that the Forchheimer number is inversely proportional to the square root of the Darcy number. The effect of inertia on heat transfer was studied for the case of $F = 0$ regardless of the

Table 1. Darcy number effect on computed average Nusselt number, $Re_D = 200$, $Pr_{eff} = 0.1$ and $Fs = 0$

Darcy number *Da*	Permeability [m²]	$\bar{h}$ [W m^{-2} K^{-1}]	$\overline{Nu}$ $\overline{Nu} = \bar{h}\, D/k_{eff}$
1×10^{-6}	2×10^{-10}	67.28	4.75
1×10^{-4}	2×10^{-8}	66.69	4.71
1×10^{-2}	2×10^{-6}	57.95	4.09
1	2×10^{-4}	44.53	3.14

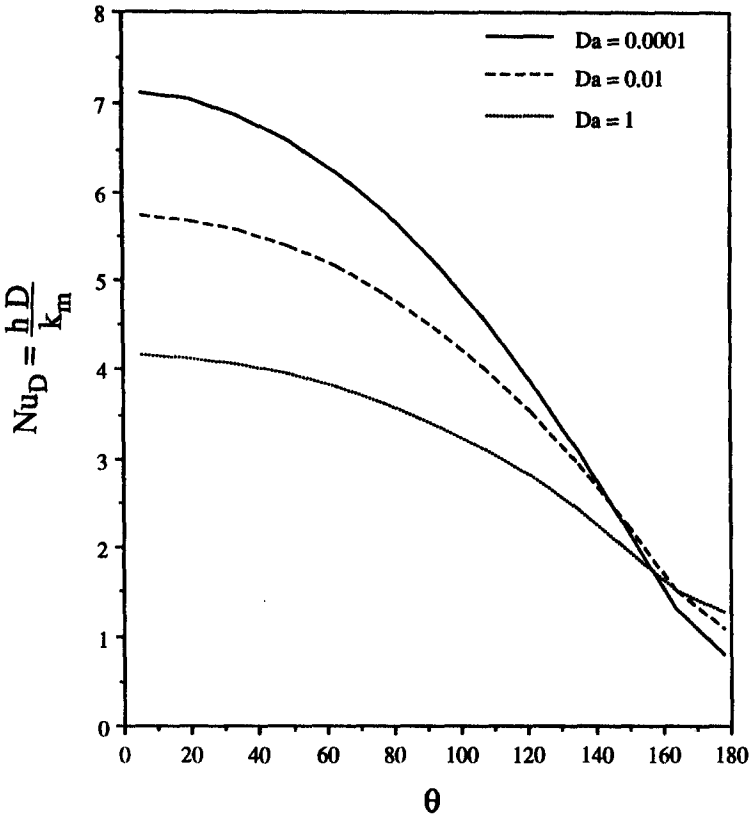

Fig. 4. Effect of Darcy number on the variation of local Nusselt number, $Re_D = 200$, $Pr_{eff} = 0.1$ and $Fs = 0$.

Darcy number; and for assigned values of *Da*, thus fixed values of *Fs*. Table 2 summarizes the computed average Nusselt numbers obtained from all simulations. The results presented in the table reveal that the Forchheimer number influences the average Nusselt number for all Darcy numbers. An interesting observation, however, is that the effect of accounting for inertia results in a slight decrease in the value of *Nu* for low *Da* numbers while the opposite is obtained for high *Da* values. From the momentum equations [equations (9) and (10)], it is observed that the product of Darcy and Reynolds numbers appears in the dimensionless Darcy term. Thus, a criterion was sought in terms of this product and in relation to the Forchheimer number. It was found that *Fs* affects *Nu* if $(Da\ Re_D) > 1 \times 10^{-4}$. Its effect results in an increase in *Nu* for $(Da\ Re_D) > 2 \times 10^{-2}$, and in a decrease in *Nu* for $(Da\ Re_D) < 2 \times 10^{-2}$. This criterion is illustrated in Fig. 5 where the ratio of average Nusselt numbers accounting for inertia (D–B–F) to those neglecting inertia (D–B) effects is plotted against the product of *Da* and Re_D.

Figure 6 illustrates the temperature profiles at an angular location of 135°. It can be seen that the temperature profiles for $Da = 1 \times 10^{-4}$, accounting and discarding inertia effects, practically coincide with each other. At $Da = 1$, the two profiles are substantially different.

Table 2. Forchheimer number effect on the average Nusselt number for various Darcy and Reynolds number values ($Pr_{eff} = 0.1$)

Darcy number	Forchheimer number	$Re_D = 200$ $\overline{Nu} = \bar{h}\,D/k_{eff}$	$Re_D = 2000$ $\overline{Nu} = \bar{h}\,D/k_{eff}$
1×10^{-6}	0	4.75	14.92
	500	4.75	13.67
1×10^{-4}	0	4.71	14.41
	50	4.60	13.90
1×10^{-2}	0	4.09	9.54
	5	4.99	19.52
1	0	3.14	6.70
	0.5	4.60	16.50

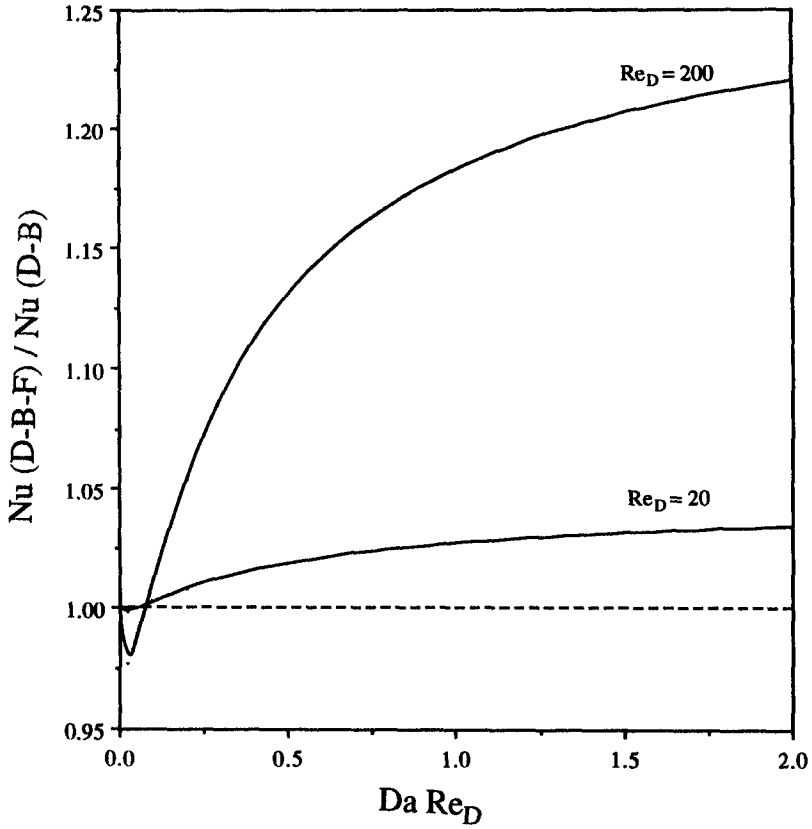

Fig. 5. Illustration of the effect of accounting for inertia effects, $Re_D = 200$ and $Pr_{eff} = 0.1$

Effect of effective Prandtl number—solid matrix

Results are presented for two different effective Prandtl number values of 0.1 and 0.03 representing glass–air and aluminum–air beds, respectively. The computed average Nusselt numbers for the two values of effective Prandtl number are 4.6 and 2.6, respectively. Thus, a three-fold increase in the effective Prandtl number results in approximately 77% increase in the average Nusselt number. The boundary layer theory predicts a Nusselt number dependence on Prandtl number to the one-half power. The ratio of the predicted Nusselt numbers (4.6/2.6 = 1.77) is close to the square root of the ratio of effective Prandtl number values (1.83) predicted by the boundary layer theory. The difference between the two cases is best illustrated in Fig. 7. It is clear that the temperature gradients are larger for the higher values of Pr_{eff}. The difference is quite substantial, particularly for θ smaller than 90°.

COMPARISON BETWEEN NUMERICAL AND EXPERIMENTAL RESULTS

Experimentally measured heat transfer coefficients for a cylinder embedded in a packed bed have been presented previously by Nasr *et al.* [8]. Numerical simulations, using a Darcy–Brinkman–Forchheimer formulation of the momentum equation, were carried out for conditions identical to those for which the experimental data were obtained. The extent of the computational domain was made to coincide with the actual dimensions of the packed bed test section used in collecting experimental data. The inlet velocity was taken to be uniform, at a constant room air temperature, and having no transverse component. A no-slip velocity boundary condition was imposed at the confining wall of the test section and on the cylinder surface. The cylinder surface temperature was taken to be 10 degrees higher than the inlet air temperature, thus simulating experimental test conditions. At the symmetry line, the gradient of the streamwise velocity component was set to zero while the transverse velocity component was constrained to be zero. Aside from the boundary conditions and thermophysical properties, input parameters such as bed porosity, inertial coefficient, and bed effective thermal conductivity are needed. Table 3 summarizes the relevant parameters for the packing types used in the experimental studies. The effective thermal conductivities are not tabulated because they were adjusted so that a match between numerical predictions and experimental data was obtained. The permeabilities of different beds are of the same order of magnitude but differ somewhat from each other due to the different particle diameters and bed porosities.

Numerical simulations may be performed for any

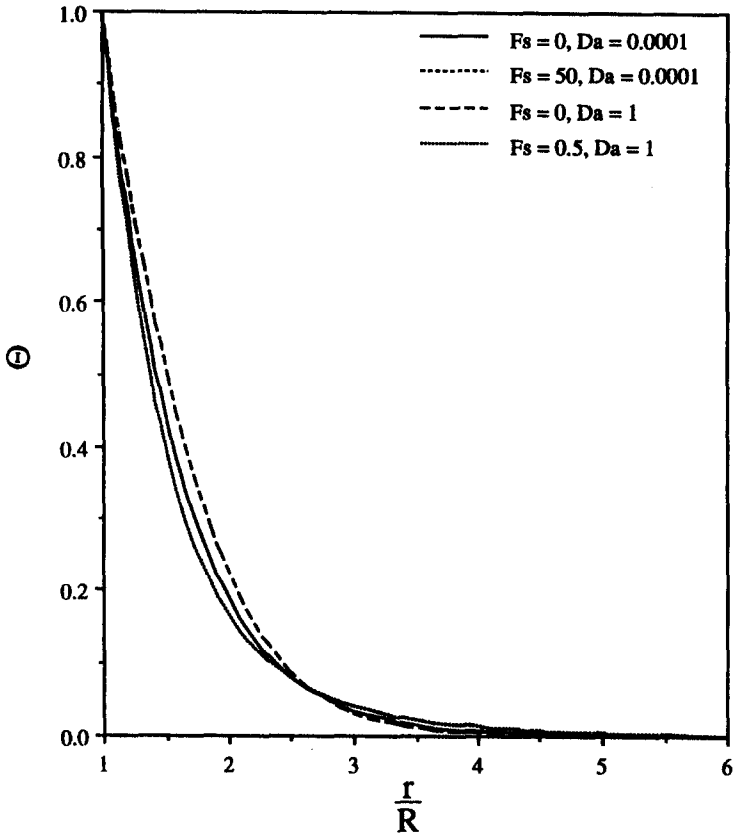

Fig. 6. Dependence of temperature profiles on Forchheimer number for two values of Darcy number ($\theta = 135°$), $Re_D = 200$ and $Pr_{eff} = 0.1$.

value of the effective thermal conductivity as an input parameter in the energy equation. However, only one value exists for k_{eff} that leads to a match between the numerically computed heat transfer coefficient and the experimentally determined value. Due to the lack of knowledge regarding effective thermal conductivities, and the absence of quantitative information on thermal dispersion effects for this physical system, the comparison presented here is for different values of k_{eff} in order to illustrate the matching process between the numerical results and their experimental counterpart.

The comparison between experimental and numerical average heat transfer coefficients must be performed on an average basis, since local heat transfer coefficients are not available. Table 4 summarizes experimental average heat transfer coefficients along with the numerically computed values under the same conditions for various systems. In this table and at a fixed fluid velocity (particle-based Peclet number), several values of effective thermal conductivity were used as input to the numerical simulation until a match with the experimental data was achieved. Therefore, for a velocity range, one would be able to compile a data set of effective thermal conductivities which produce a match between numerical and experimental results. This set will be used as a basis for the quantification of thermal dispersion as presented in the next section.

THERMAL DISPERSION

It is known that the effective thermal conductivity of packed beds is enhanced if thermal dispersion effects are present (Kuo and Tien [20]; Cheng and Vortmeyer [21]). Thermal dispersion is a result of the simultaneous existence of temperature and velocity gradients within the pores of the porous medium. An attempt to quantify its contribution to heat transfer from an embedded cylinder is presented here.

The effective thermal conductivity may be considered to be a superposition of a stagnant conductivity (independent of flow) and a flow-dependent dispersion conductivity. The matching process between experimental and numerical results yielded the total effective thermal conductivities. Figure 8 presents the ratio of the effective thermal conductivity to the fluid thermal conductivity against the particle-based Peclet number for various packed beds. The effective thermal conductivity shows a dependence on the Peclet number that is fairly linear. Several observations regarding the slope and y-intercept of each data set can be made from this figure. It is seen that the 6 mm nominal diameter glass and nylon beds have

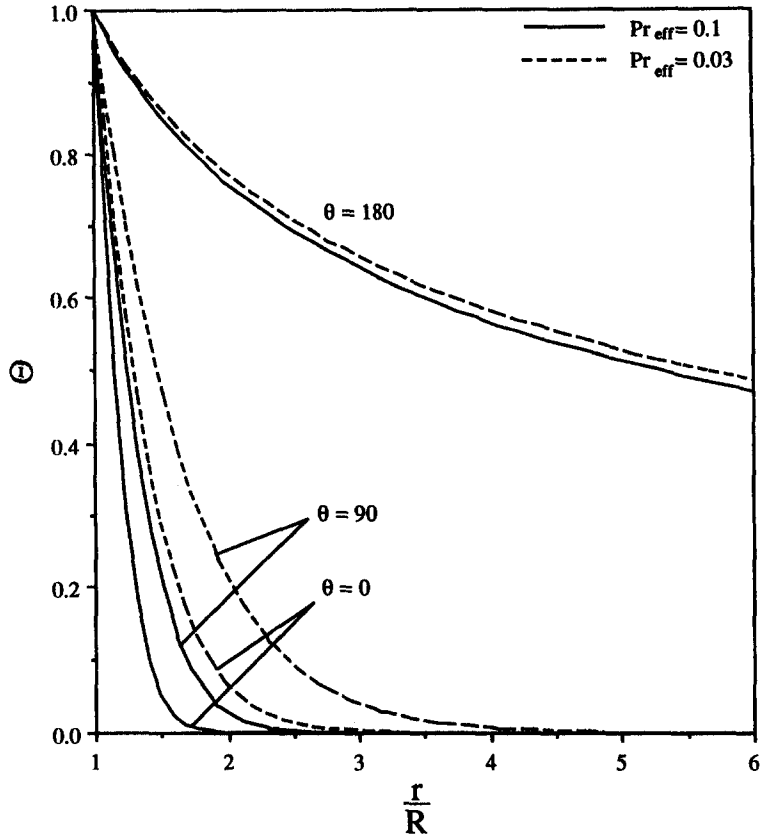

Fig. 7. Comparison of temperature profiles for two different values of effective Prandtl number, $Re_D = 200$, $Da = 1 \times 10^{-4}$, and $Fs = 50$.

practically the same slope and y-intercept, and that the same holds true for the 13 mm nominal diameter glass and nylon beds. A clear dependence on the particle diameter is displayed, while the y-intercept appears to be independent of the solid thermal conductivity for the glass and nylon beds. In addition, the y-intercept for the 13 mm data falls substantially below those for the 3 and 6 mm. A possible explanation is that the 13.53 mm glass particles and 12.7 mm nylon particles are as large as the cylinder diameter (12.7 mm), suggesting that the continuum treatment to the problem is inappropriate and volume averaging is not suitable. The dependence of the effective thermal conductivity on the solid thermal conductivity becomes significant when comparing the high conductivity bed (aluminum) with the low conductivity bed (glass).

For the quantification of thermal dispersion, a stagnant conductivity value is needed. Various models for the quantification of the stagnant thermal conductivity exist in the literature. An extensive comparison of the models' predictions is presented in Nasr [18]. The model of Zehner and Schlünder [19] is considered as well established but predicts higher values

Table 3. Relevant parameters used for the numerical studies for the purpose of comparison with experimental data

Material	d_p [mm]	ϕ [%]	K [m^2] $\times 10^{-8}$	F	$Da \times 10^{-4}$	Fs
Aluminum	3.24	0.37	0.59	0.48	0.37	78
	6.33	0.38	2.5	0.46	1.58	36
	12.23	0.39	10.6	0.44	6.57	17
Alumina	2.77	0.36	0.39	0.50	0.24	101
	6.64	0.37	2.5	0.48	1.55	38
	9.62	0.38	5.8	0.46	3.63	24
Glass	2.85	0.37	0.46	0.48	0.28	89
	6.00	0.37	2.0	0.48	1.27	42
	13.53	0.39	13.0	0.44	8.04	15
Nylon	6.35	0.37	2.3	0.48	1.42	40
	12.7	0.39	11.4	0.44	7.09	16

Table 4. Comparison of experimental and numerical results for various input values of the effective thermal conductivity

U_∞ [m s^{-1}]	Pe_p	$\bar{h}_{Exp.}$ [W m^{-2} K^{-1}]	k_{eff} [W m^{-1} K^{-1}]	Pr_{eff}	$\bar{h}_{Num.}$ [W m^{-2} K^{-1}]	$\overline{Nu}_{Exp.} = \bar{h}_{Exp.}D/k_{eff}$	$\overline{Nu}_{Num.} = \bar{h}_{Num.}D/k_{eff}$
0.21	27	57.67	0.180	0.103	52.00	4.07	3.67
[glass			0.205	0.091	55.97	3.57	3.47
2.85 mm]			**0.216**	0.086	**57.67**	3.39	3.39
2.41	643	224.16	0.240	0.077	218.99	11.86	11.59
[glass			0.248	0.075	222.68	11.48	11.40
6.00 mm]			**0.251**	0.074	**224.16**	11.34	11.34
2.4	678	214.41	0.260	0.071	227.36	10.47	11.10
[nylon			0.235	0.079	217.48	11.59	11.75
6.35 mm]			0.227	0.082	213.21	12.00	11.93
			0.229	0.081	**214.41**	11.89	11.89

(approx. 20%) of the stagnant conductivities than those obtained by extrapolation to zero Pe_p values. In the present situation, the diameter of the cylinder is comparable to the diameter of the particles. This situation differs considerably from the experimental arrangements used in developing models for the stagnant conductivity. Thus, it is believed that an extrapolation to zero value of Pe_p is an appropriate procedure for determining the stagnant conductivity. Considering the y-intercept of the best-fit line through the data for the effective thermal conductivity as the stagnant conductivity, the dispersion conductivity may be calculated as the difference between the total (effective) and the stagnant values. Numerous investigators (Yagi and Kunii [22]; Cheng *et al.* [23]), found that the average value of the dispersive conductivity in internal flow configurations may be correlated as a linear function of the particle-based Peclet number,

$$k_{disp} = C_{disp} k_f Pe_p \tag{12}$$

where k_{disp} is the dispersive thermal conductivity, Pe_p is the particle-based Peclet number and C_{disp} is the coefficient of thermal dispersion or thermal dispersivity. In the present study, the coefficient of thermal dispersion was found to be a function of particle-to-cylinder diameter ratio. This dependence may be correlated for all packing materials by

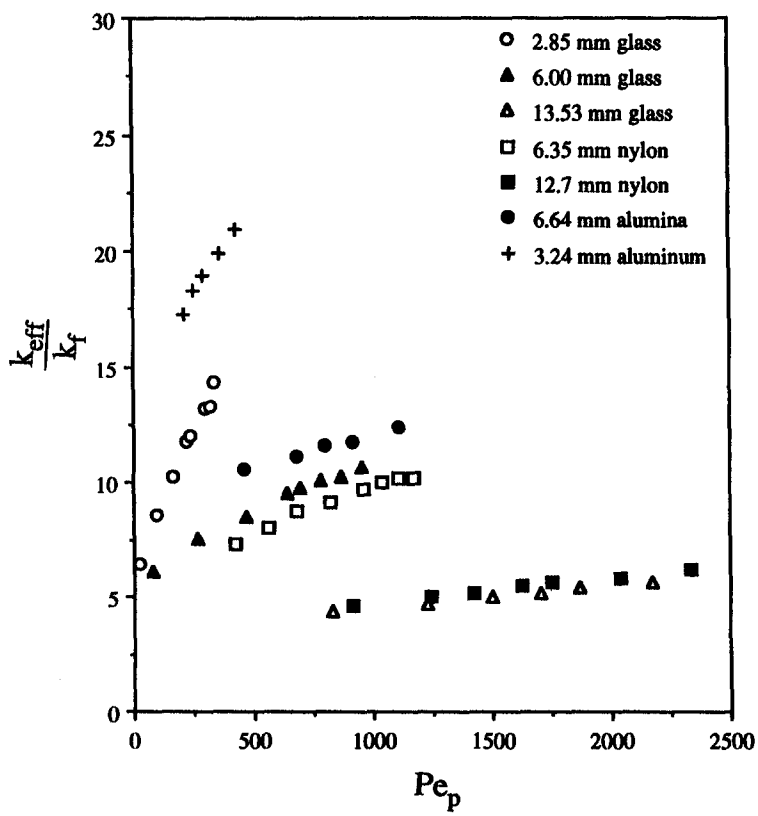

Fig. 8. Dependence of effective thermal conductivity on the particle-based Peclet number.

$$C_{\text{disp}} = c_1 \left(\frac{d_p}{D}\right)^{c_2} \tag{13}$$

where c_1 and c_2 are empirical constants obtained by least-squares fitting of the data. Performing such a fit led to values of 1.02×10^{-3} and -2.0 for c_1 and c_2, respectively. On substituting equation (13) into equation (12), the following empirical correlation for k_{disp} is obtained:

$$k_{\text{disp}}/k_f = 1.02 \times 10^{-3} \left(\frac{d_p}{D}\right)^{-2.0} Pe_p. \tag{14}$$

In order to affirm that such a form is suitable for all the packings examined in this study, Fig. 9 plots the correlated values, predicted by equation (14), against the measured values obtained from $(k_{\text{eff}} - k_o)/k_f$, where k_o is a y-intercept value of the line plotted through each data set shown in Fig. 8. In addition, Fig. 10 shows the magnitude of the dispersive to fluid conductivity ratio as a function of the Peclet number. It is seen that the dispersive conductivities for the 3 mm nominal particle diameter are essentially the same for glass and aluminum particles. The same observation can be made regarding the 6 and 13 mm nominal particles. The dispersive conductivity is shown to be independent of the packing material, but exhibits a strong dependence on the particle size.

CONCLUSIONS

In this paper, heat transfer from an embedded cylinder was studied numerically. The effects of governing dimensionless parameters were presented. The local volume-averaged equations, accounting for viscous and inertia (non-Darcian) effects, were later used to compare the numerical predictions with experimental data and to deduce the contribution of thermal dispersion to the total effective thermal conductivity.

Based on the numerical results obtained, an increase in Reynolds number was found to enhance heat transfer. This enhancement was found to be consistent with that obtained from the predictions of the boundary layer theory, which shows a Nusselt number dependence on the Reynolds number to the one-half power. The effect of increasing Darcy number was found to yield a decrease in heat transfer. An increase in Da by four orders of magnitude resulted in approximately 35% decrease in Nu. Although the decrease in the Darcy number provided an increase in the Nusselt number, the rate of this increase in Nu was found to decrease with decreasing values of Da. The Forchheimer number influences the average Nusselt number and its effect depends on the magnitude of the product of Da and Re_D. The effect of retaining the inertia terms in the momentum equation yields an increase in Nu

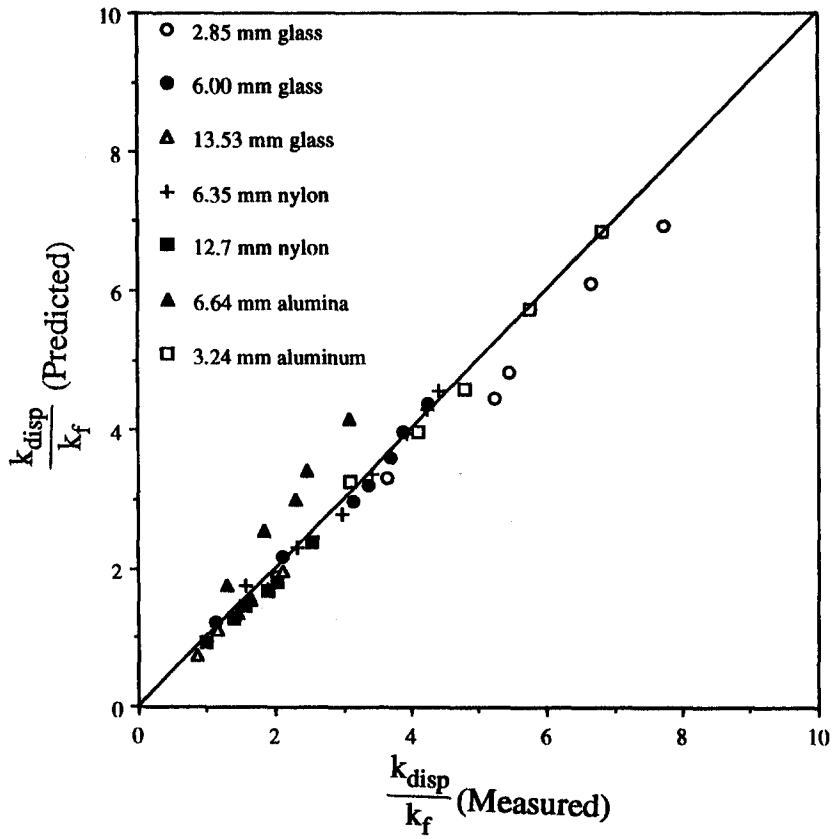

Fig. 9. Predicted vs measured values of the dispersive-to-fluid conductivity ratios for different packed beds.

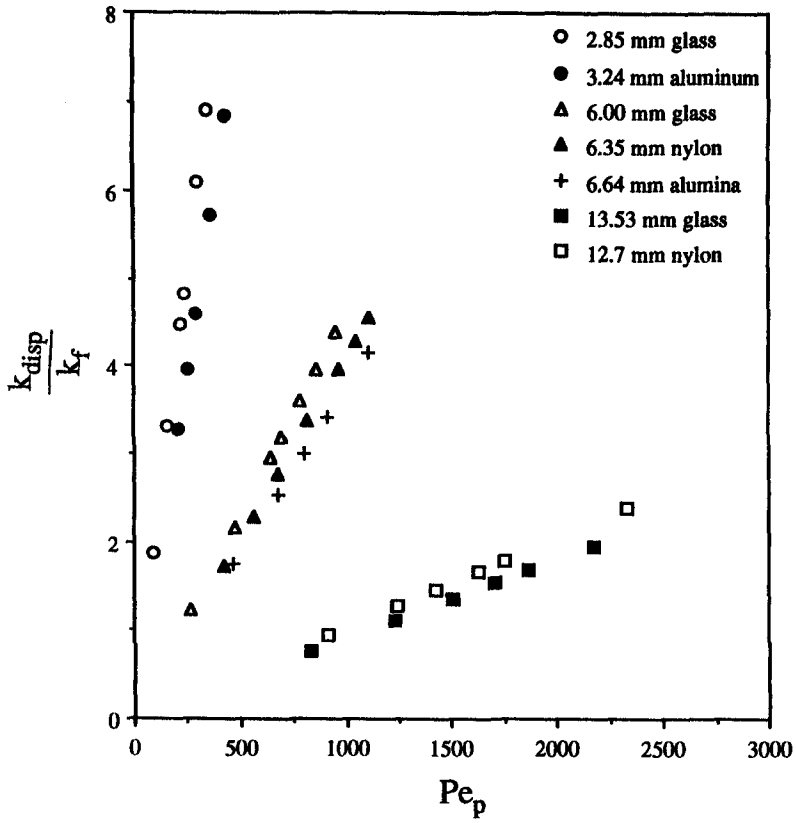

Fig. 10. Ratio of dispersive conductivity to fluid conductivity for various packed beds.

for $(Da\ Re_D) > 2 \times 10^{-2}$ and a slight decrease for $(Da\ Re_D) < 2 \times 10^{-2}$. As for the influence of the effective Prandtl number, the Nusselt number increases with the Prandtl number, and this increase is close to that predicted by the boundary layer theory.

The effective thermal conductivity, taken to be the sum of the stagnant (independent of flow conditions) effective conductivity and of the dispersive (flow-dependent) conductivity, was extracted by comparing the model predictions with available experimental data. The contribution due to thermal dispersion was correlated in terms of the particle-based Peclet number, for which the average coefficient of thermal dispersion was found to depend on the particle-to-cylinder diameter ratio.

It is noted that thermal dispersion effects were deduced as a result of a comparison made between cylinder-average numerical and experimental results. Local effects, mainly accounting for porosity variation and regarding the effective thermal conductivity as a local function of relevant variables need to be investigated in future studies.

REFERENCES

1. P. Cheng, Mixed convection about a horizontal cylinder and a sphere in a fluid-saturated porous medium, *Int. J. Heat Mass Transfer* **28,** 1245–1247 (1982).
2. W. Minkowycz, P. Cheng and C. Chang, Mixed convection about a nonisothermal cylinder and a sphere in a porous medium, *Numer. Heat Transfer* **8,** 349–359 (1985).
3. M. Huang, K. Yih, Y. Chou and C. Chen, Mixed convection flow over a horizontal cylinder or a sphere embedded in a saturated porous medium, *J. Heat Transfer* **108,** 469–471 (1986).
4. H. Badr and I. Pop, Combined convection from an isothermal cylinder rod buried in a porous medium, *Int. J. Heat Mass Transfer* **31,** 2527–2541 (1988).
5. V. Murty, C. Clay, M. Camden and D. Paul, A study of non-Darcian effects on forced convection heat transfer over a cylinder embedded in a porous medium, *Heat Transfer* **5,** 201–206 (1990).
6. R. M. Fand and R. T. Phan, Combined forced and natural convection heat transfer from a horizontal cylinder embedded in a porous medium, *Int. J. Heat Mass Transfer* **30,** 1351–1358 (1987).
7. R. M. Fand, M. Varahasamy and L. S. Greer, Empirical correlation equations for heat transfer by forced convection from cylinders embedded in porous media that account for the wall effect and dispersion, *Int. J. Heat Mass Transfer* **36,** 4407–4418 (1993).
8. K. Nasr, S. Ramadhyani and R. Viskanta, An experimental investigation on forced convection heat transfer from a cylinder embedded in a packed bed, *J. Heat Transfer* **116,** 73–80 (1994).
9. J. C. Slattery, Two-phase flow through porous media, *A.I.Ch.E. Jl* **16,** 345–352 (1970).
10. K. Vafai and C. L. Tien, Boundary and inertia effects on flow and heat transfer in porous media, *Int. J. Heat Mass Transfer* **24,** 195–203 (1981).
11. R. G. Carbonell and S. Whitaker, Heat and mass transfer in porous media. In *Fundamentals of Transport Phenomena in Porous Media* (Edited by J. Bear and M. Y. Con-

apcioglu), pp. 121–198. Martinus Nijhoff, Dordrecht, The Netherlands (1984).
12. C. Hsu and P. Cheng, Thermal dispersion in a porous medium, *Int. J. Heat Mass Transfer* **33,** 1587–1597 (1990).
13. M. Kaviany, *Principles of Heat Transfer in Porous Media*. Springer, New York (1991).
14. G. Lauriat and K. Vafai, Forced convective flow and heat transfer through a porous medium exposed to a flat plate or a channel. In *Convective Heat and Mass Transfer in Porous Media* (Edited by S. Kakaç, B. Kilkis, F. Kulacki and F. Arinç), pp. 289–327. Kluwer Academic Publishers, Dordrecht, The Netherlands (1991).
15. D. A. Nield and A. Bejan, *Convection in Porous Media*. Springer, New York (1992).
16. S. Ergun, Fluid flow through packed columns, *Chem. Engng Prog.* **48,** 89–94 (1952).
17. Fluid Dynamics International (FDI), *Fluid Dynamics Analysis Package—Theory Manual*, Evanston, Illinois (1993).
18. K. J. Nasr, Experimental and numerical studies of forced convection and radiation heat transfer in packed beds, Ph. D. Thesis, Purdue University, West Lafayette, Indiana (1993).
19. P. Zehner and E. U. Schlünder, Thermal conductivity of granular materials at moderate temperatures, *Chem. Ingr. Tech.* **42,** 933–941 (1970) (in German).
20. S. M. Kuo and C. L. Tien, Transverse dispersion in packed-spheres beds, *ASME Proceedings of the* 1988 *National Heat Transfer Conference*, HTD 96, pp. 629–634. ASME, New York (1988).
21. P. Cheng and D. Vortmeyer, Transverse thermal dispersion and wall channelling in a porous bed with forced convective flow, *Chem. Engng Sci.* **9,** 2523–2532 (1988).
22. S. Yagi and D. Kunii, Studies on heat transfer near wall surface in packed beds, *A.I.Ch.E. Jl* **6,** 97–104 (1960).
23. P. Cheng, A. Chowdhury and C. T. Hsu, Forced convection in packed tubes and channels with variable porosity and thermal dispersion effects. In *Convective Heat and Mass Transfer in Porous Media* (Edited by S. Kakaç, B. Kilkis, F. Kulacki and F. Arinç), pp. 625–654. Kluwer Academic Publishers, Dordrecht, The Netherlands (1991).